

## Capacity and the moment-curvature relationship of high-strength concrete filled steel tube columns under eccentric loads

Seung-Jo Lee\*

Beom Structural Engineering Co., 675-9 2F Hwanggeum 2-dong, Suseong-gu,  
Daegu 706-852, Korea

(Received August 2, 2006, Accepted March 7, 2007)

**Abstract.** Recently, CFT column has been well-studied and reported on, because a CFT column has certain superior structural properties as well as good productivity, execution efficiency, and improved rigidity over existing columns. However, CFT column still has problems clearing the capacity evaluation between its steel tube member and high-strength concrete materials. Also, research on concrete has examined numerical values for high-strength concrete filled steel square tube columns (HCFT) to explain transformation performance ( $M-\phi$ ) when a short-column receives equal flexure-moment from axial stress. Moment-curvature formulas are proposed for HCFT columns based on analytic assumption described in this paper. This study investigated structural properties (capacity, curvature), through a series of experiments for HCFT with key parameters, such as strength of concrete mixed design (58.8 MPa), width-thickness ratio ( $D/t$ ), buckling length to sectional width ratio ( $L_b/D$ ) and concrete types (Zeolite, Fly-ash, Silica-fume) under eccentric loads. A comparative analysis executed for the AISC-LRFD, AIJ and Takanori Sato, etc. Design formulas to estimate the axial load ( $N$ )-moment ( $M$ )-curvature ( $\phi$ ) are proposed for HCFT columns based on tests results described in this paper.

**Keywords:** high-strength concrete filled steel square tube column;  $D/t$  ratio; buckling length to sectional ratio; eccentric ratio; axial load capacity ratio; curvature; ductility.

### 1. Introduction

Currently, the concrete filled steel tube column (CFT) for high-rise buildings is highly popular as it provides lots of benefits such as better structural capacities than the reinforced concrete (RC) or steel column, as well as workability and fire resistance. Many experimental investigations on CFT columns were conducted by Inai *et al.* (2004), Uy (2003), Sakino *et al.* (2004), Campione and Scibilia (2002), Young and Lui (2005), Liu *et al.* (2003), Han and Yao (2003) and many other researchers. Saito *et al.* (1989) extensively investigated the behavior of both circular and square CFT beam columns with 490 and 570 MPa steel tube and 27 to 63 MPa concrete. Itoh and Yasuzaki (1992), and Inoue *et al.* (1994) investigated the behavior of CFT beam columns with high-strength materials including 780MPa steel tubes. These databases indicate that experimental data is lacking for square CFT columns made from high-strength concrete types (Zeolite, Fly-ash, and Silica-fume) and high-strength steel subjected to

---

\*Ph.D., Senior Engineer

constant eccentric load. Due to the lack of this knowledge, most design code provisions restrict the use of high-strength steel and concrete in CFT columns. Research interest in CFT columns made from high-strength materials has increased worldwide. Also, most existing studies have carried out analytic research focused on the behavior of normal concrete for CFT, or analysis and design of CFT using analytic methods. Up to now, most CFT designs have been based on the strength of normal concrete (Knowles *et al.* 1969). Studies on the properties of concrete for CFT or designs for high-strength concrete are insufficient as they are still in research. Demands for high-rise buildings in future require high-strength steel and concrete, the main components of CFT, and structural stability. Understanding the structural properties of both high-strength concrete and CFT are indispensable to establish a design for HCFT column. Consequently, this study is intended to investigate the effect of HCFT column on axial load-moment ( $N-M$ ) capacity interaction curves and buckling strength. Experiments involving five multiple variables carry out a numerical analysis of the moment-curvature ( $M-\phi$ ) relation for the deformational properties of the short column applied by equal bending moment under axial load ( $N$ ). The test results are compared with the design rules given in various codes AISC-LRFD (2005), CFT recommendations (1997) and SRC standards (1987) by AIJ and a proposal by Sato (1999).

## 2. Experiment outline and plan

### 2.1 Specimen plan

Specimens are fabricated SS400 type square steel tubes with  $\square$ -75 $\times$ 75 $\times$ 3.2,  $\square$ -100 $\times$ 100 $\times$ 3.2 and  $\square$ -100 $\times$ 100 $\times$ 2.3(mm) and 23.4, 33.3 and 43.5 of width-thickness ratios ( $D/t$ ) respectively. High-strength concrete with  $f_c = 58.8$  MPa of compressive strength is used for CFT. Three types of buckling length to sectional width ratio ( $L_k/D = 4, 8$  and  $12$ ), four types of eccentricity ratio ( $e = 0.0, 0.1, 0.2$  and  $0.3$ ) and Zeolite (A), Fly ash (B) and Silica-fume (C) for concrete for CFT are selected for experiment variables and a total of 108 specimens are made.

### 2.2 Test set-up

For the eccentric load column test, a hydraulic universal testing machine 1976.19 kN capacity (U.T.M) is used, and Fig. 1 shows schematic of column test set-up. Linear varying displacement transducers (LVDT's) were used to measure the displacement of the column at the mid height and at the end points of the column. The location of the six LVDT's is illustrated in Fig. 1. Strain gauges were used to measure the surface strains of the steel section at the mid height section at horizontal locations and vertical.

### 2.3 Material property test

#### 2.3.1 Tensile test of material

Material property tests were carried out before the column tests. Specimens for a tensile test of steel (SS400) are fabricated in accordance with Korean standard (KS B 0801) regulations for specimens for a tensile test of metallic materials (No.7), and the test is carried out subject to KS B 0802, tensile test method of metallic material piece. Wire strain gauges (W.S.G) are attached to the both sides of a specimen, and the results estimated by mean values are shown in the Table 1.

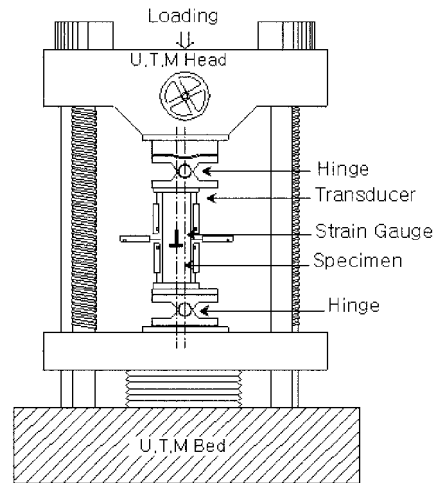


Fig. 1 Schematic of column test set-up

Table 1 Test results of tension

Specimen	$F_y$ (MPa)	$F_{max}$ (MPa)	$F_{max}/F_y$	$E_s$ (MPa)	$Elo$ (%)
□ - 75×75×3.2	347.6	432.6	0.799	232554	23.7
□ - 100×100×3.2	364.1	435.0	0.836	215894	21.4
□ - 100×100×2.3	366.8	464.8	0.796	202272	22.1

Table 2 Test results of compressive strength

$f_c$ (MPa)	Slump (mm)	Unit weight (N/m <sup>3</sup> )						$f_{cu}$ (MPa)	$\varepsilon$ (%)
		Cement	Admixture	Sand	Gravel	Water	Agent		
58.8	130	4707.1	519.7	7296.1	9129.9	1569	78.4	54.3	0.31

### 2.3.2 Compressive strength test of concrete

Nine specimens were fabricated for a strength test in accordance with KS F 2404 regulations, and a compressive strength test was carried out. Table 2 shows the mixing design of the concrete and test results.

## 3. Test results and discussions

### 3.1 Load-displacement curves

All of the tested curves of load versus displacement are shown in Figs. 2(a) to 2(i). While the curves tend to drop quickly after the peak load for the specimen, the load tends to maintain after the peak. The ultimate axial load capacity ( $N$ ) obtained in the test is summarized in Table 4. A careful examination of the test results revealed an interesting phenomenon, i.e., in the initial elastic stage, the lateral strain of the Zeolite (A), Fly-ash (B) was almost the same as that of the Silica-fume (C) specimen. In addition, the initial elastic stage tends to increase as width-thickness ratio ( $D/t$ ) and buckling length-sectional

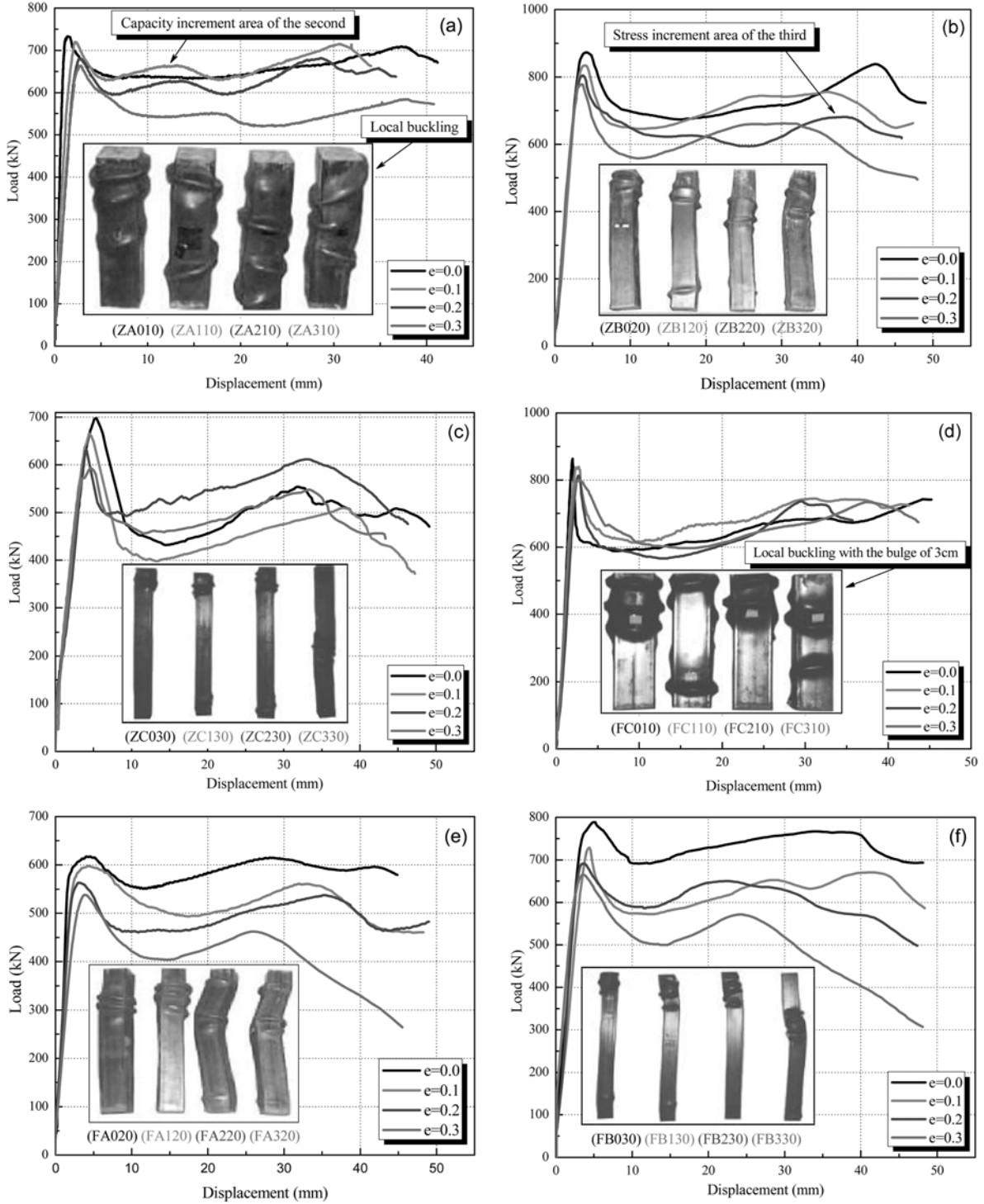


Fig. 2 Experimental curves of load versus axial displacement

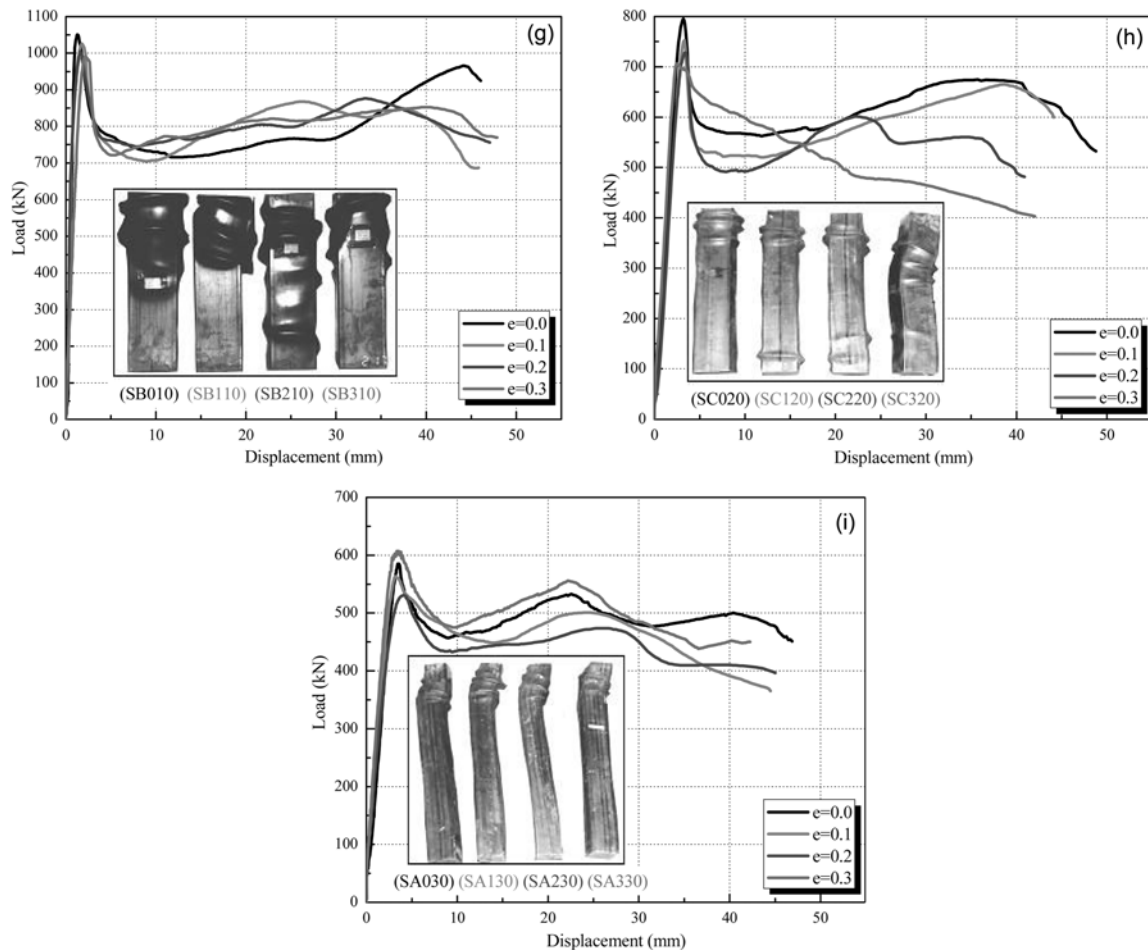


Fig. 2 (Continued) Experimental curves of load versus axial displacement and failure modes

width ratio ( $L_k/D$ ) decreases. Mostly, the axial load ( $N$ ) decreased the capacity of the short column ( $L_k/D = 4$ ) in the upper and lower parts of specimen, and the buckling in the behavior phenomenon occurred after reaching maximum capacity.

The capacity decreased rapidly as the eccentric ratio ( $e$ ) and  $D/t$  ratio decreased. The primary capacity decreased to from 10 to 40% extent of maximum capacity. It is notable that the rate for the Silica-fume (C) concrete for CFT was higher than for the Zeolite (A) and Fly-ash (B) concrete for CFTs as the  $D/t$  ratio increased. The short column shows the second capacity increment curve after primary capacity reduction. The secondary stress region is ascending to from 80 to 95% of maximum capacity according to eccentric ratio ( $e$ ) and its value. The increasing rate of the Zeolite (A) concrete for CFT was significantly greater than that of the other specimen as the load increased.

In addition, the long column specimen ( $L_k/D = 8, 12$ ) reduced capacity, generating by local buckling generally in the specimen's central part. The capacity decrease was slow compared to that of the short column and low, between 10 and 30% extents. However, the specimen showed unstable behavior: the capacity rising curve was three to four times that of the secondary capacity rising curve in the case of the short column.

### 3.2 Failure modes

#### 3.2.1 Failure modes of concrete admixture for CFT

Typical failure mode was a local (outward folding) failure mechanism. This is the same as that observed by other researchers (Varma *et al.* 2004) for CFT sections. Typical failure mode of the tested specimens is shown in Figs. 2(a) to 2(i).

##### 3.2.1.1 Zeolite concrete for CFT

The steel tube bulged through lateral expansion of the inner concrete regardless of  $D/t$  ratio in the  $L_k/D = 4$ . As shown in Fig. 2(a), the specimen moved from the upper point to the center as the eccentric ratio ( $e$ ) increased in the compressive failure. The  $D/t = 23.4$  failure began with the local buckling of the steel tube between the upper part and the lower at the 1/4 zone, as shown in Fig. 2(b). Because of the infill concrete the buckled flanges and the tube webs all deformed outwards. The failure mode became more noticeable as the eccentric ratio ( $e$ ) increased. The failure modes for specimen  $D/t = 23.4$  of  $L_k/D = 12$  were similar to that of specimen  $L_k/D = 8$ . The local buckling position tended to move from the upside to the middle. The  $D/t = 33.3, 43.5$  was observed with a local buckling at the middle of specimen.

##### 3.2.1.2 Fly-ash and silica-fume for CFT

The Fly-ash (B) and Silica-fume (C) specimen for CFT tended to be similar to the Zeolite (A) specimen in the  $L_k/D = 4, L_k/D = 12$ . In the case of  $D/t = 23.4$  for  $L_k/D = 8$ , the B and C specimens had a larger local buckling and failure modes than the A specimens. The effect of local buckling appeared more often as the eccentric ratio increased. For a decreasing eccentric ratio ( $e$ ), the  $D/t = 33.3, 43.5$  specimens have a tendency to burst due to bulging of the steel tube. These B and C specimens showed a rapid reduction in concrete after maximum axial load capacity was attained. The specimens with  $D/t = 33.3, 43.5$  were subjected to large axial load but only a small confining effect.

In spite of the large axial load which acted on HCFT section as a result of the high-strength of the concrete, the deterioration of the load-bearing capacity of the concrete could not be adequately constrained due to the insufficient strength of the steel tube which has the function of constraining the concrete.

#### 3.2.2 Failure mode of crushing concrete

Fig. 3 shows the crushing of concrete admixture under the region where the locally buckled tube had been removed. The inner failure mode of the Zeolite (A) of  $D/t = 23.4$  was bulging at the upper, where the specimen failure mode became a hollow in  $L_k/D = 4$ . This part of the concrete was separated from steel tube, where the specimen had failure in general. The failure modes became more noticeable as the eccentric ratio ( $e$ ) increased and spread to the mid region. Also, the specimen was observed with minute cracks at the mid to lower regions in  $L_k/D = 4$ . The  $D/t=33.3$  has a tendency similar to  $D/t = 23.4$  with the horizontal crack. Comparison between specimens  $D/t = 43.5$  and  $D/t = 23.4, 33.3$  illustrates that the inner failure mode became greater as the  $D/t$  ratio increased in the failure of concrete and mixed horizontal-diagonal of crack, as shown in Fig. 3. The case of the  $D/t = 43.5$  specimen shows many minute cracks before maximum capacity was reached, due to the lateral expansion of the steel tube from the axial load being applied on the concentrated concrete part. The B and C specimens are similar to the Zeolite (A) CFT in failure mode.

The failure mode of the concrete for the B and C specimens, however, was observed to be larger than

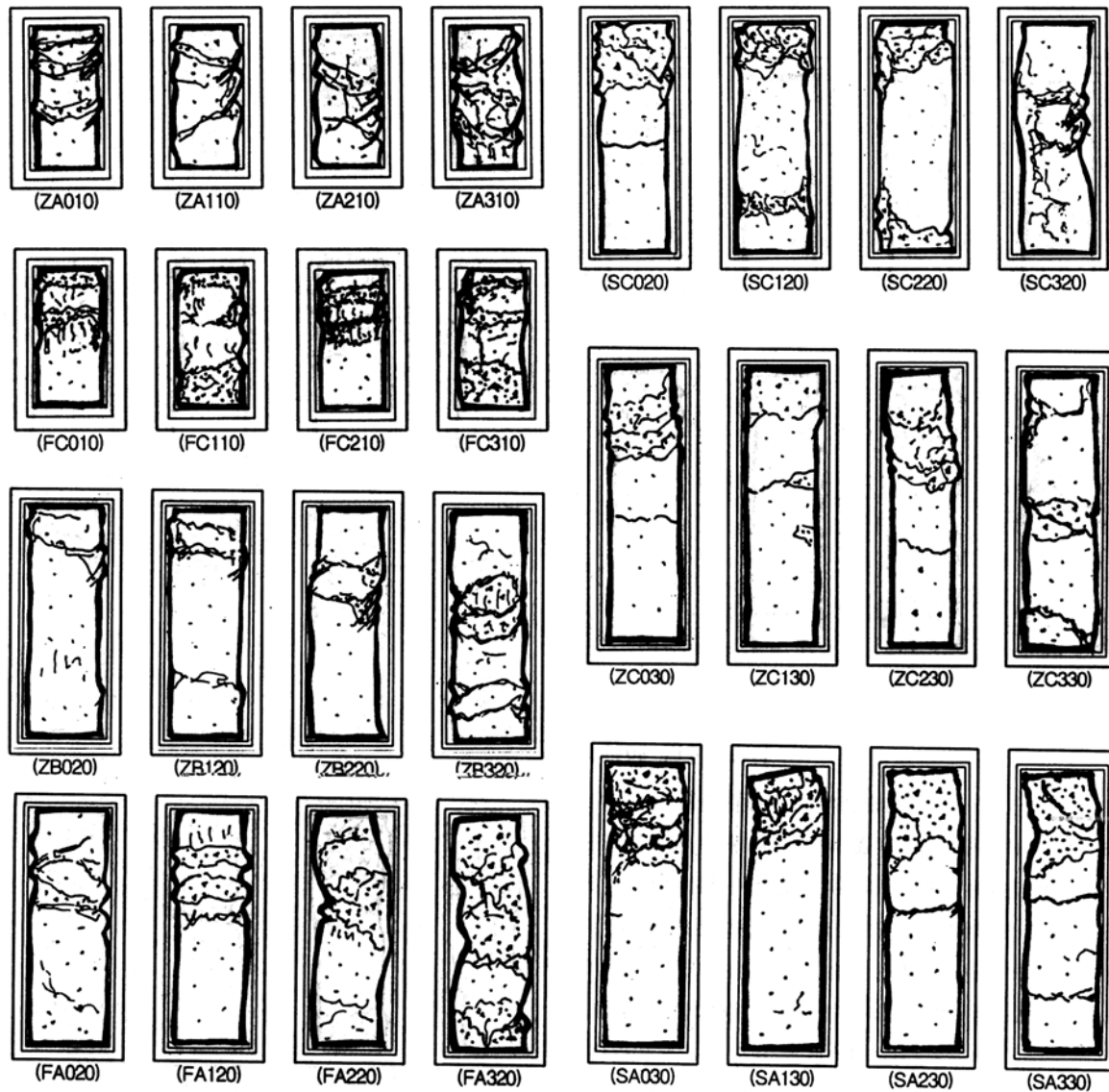


Fig. 3 Failure mode of crushing concrete

for the A, and the concrete was separated from the steel tube. The effect of the buckling length-sectional width ratio ( $L_k/D$ ) and the  $D/t$  ratio on a crack's appearance was most significant. This parameter indicates that tubes with excessive  $D/t$  ratio and  $L_k/D$  should be avoided in HCFT design so that tube fracturing can be prevented and member performance can be sustained. The failure of the concrete and a separated appearance from the steel tube was observed in  $D/t = 23.4$ , at a compressive failure point and local buckling, regardless of the concrete types used for CFT in the  $L_k/D = 8$ . For the shape of the inner failure, the  $D/t = 33.3, 43.5$  has a tendency similar to  $D/t = 23.4$  with the horizontal and diagonal cracks. There is no observable shape for failure of concrete from the upper to lower areas of the specimen. Regardless of the concrete used for CFT, the crack illustrates that the mixed cracking

occurs at a local buckling point as shown in Fig. 3.

### 3.3 Ductility

The ductility performance was compared using the displacement ductility. The displacement ductility is defined as the ratio between displacements at the ultimate and yielding points, expressed in the following:

$$\Delta = \Delta_u / \Delta_y \quad (1)$$

In which  $\Delta_y$  is the yielding displacement and  $\Delta_u$  is the displacement at the ultimate stage, determined by the value when the member strength dropped to 90% of its maximum strength. This criterion was set to reflect the member's inelastic deformation capability. The influence of the width to thickness ( $D/t$ ) ratio, the buckling length to sectional width ( $L_k/D$ ) ratio and the eccentricity ( $e$ ) ratio of the steel tube on the ductility ( $\Delta$ ) of the HCFT specimens is shown in Fig. 4. Fig. 4(a) indicates that increasing the width to thickness ( $D/t$ ) ratio reduces the ductility ( $\Delta$ ). It is shown from the comparisons that the improvement in displacement ductility was most significant in members with  $D/t$  ratios equaling 23.4. The highest displacement ductility improvement for this test series was 31.4%. For members with larger  $D/t$  ratios, i.e., 33.3 and 43.5 test series, the performance gains were less than the above test series, however, they still exhibited 29.4% and 24.3% improvements. This phenomenon could be attributed to the plate stability because the member performance was governed by the formation of a plastic hinge at the locally buckled region. When the members were composed of steel tubes with a smaller  $D/t$  ratio, the thicker plates were capable of dissipating more energy without significant strength loss; therefore, stable hysteretic behavior and higher ductility performance could be displayed. However, the buckled thin steel tubes would easily reach the fracture stage, causing leakage of crushed infilled concrete and distortion in the steel tube sections.

Fig. 4(b) indicates that increasing the buckling length to sectional width ( $L_k/D$ ) ratio also significantly reduces the ductility ( $\Delta$ ) with A-specimen. The reduction of ductility ( $\Delta$ ) in Fig. 4(b) is larger for specimens with a lower buckling length to sectional width ( $L_k/D$ ) ratio (i.e. with  $L_k/D = 8$ ). For members with a buckling length to sectional width ( $L_k/D$ ) ratios equaling 4, 8, and 12, the maximum performance gains in ductility were 27.5%, 22.9%, and 34.8%, respectively. Fig. 4(c) indicates that the eccentricity ( $e$ ) ratio of the specimen, generally, has a small influence on the ductility. The eccentricity ratios of the steel tube have a small influence on ductility ( $\Delta$ ) of the specimens subjected to higher eccentricity 0.3.

## 4. Comparison of test results with capacity predictions based on current code provisions

### 4.1 AISC-LRFD ( $N_L$ )

Generally, American designers select and reflect American Concrete Institute code (ACI 318-2005) and AISC-LRFD (2005) for the examination of CFT structures. For this standard, the Architectural Institute of Korea design (AIK 2004) for composite columns has been encased by RC such as H-beam shape and square steel tube or circular steel tube infill with concrete. Those contents are similar to that stated in previous AISC-LRFD provisions. Therefore, this paper investigates only AISC-LRFD (2005).

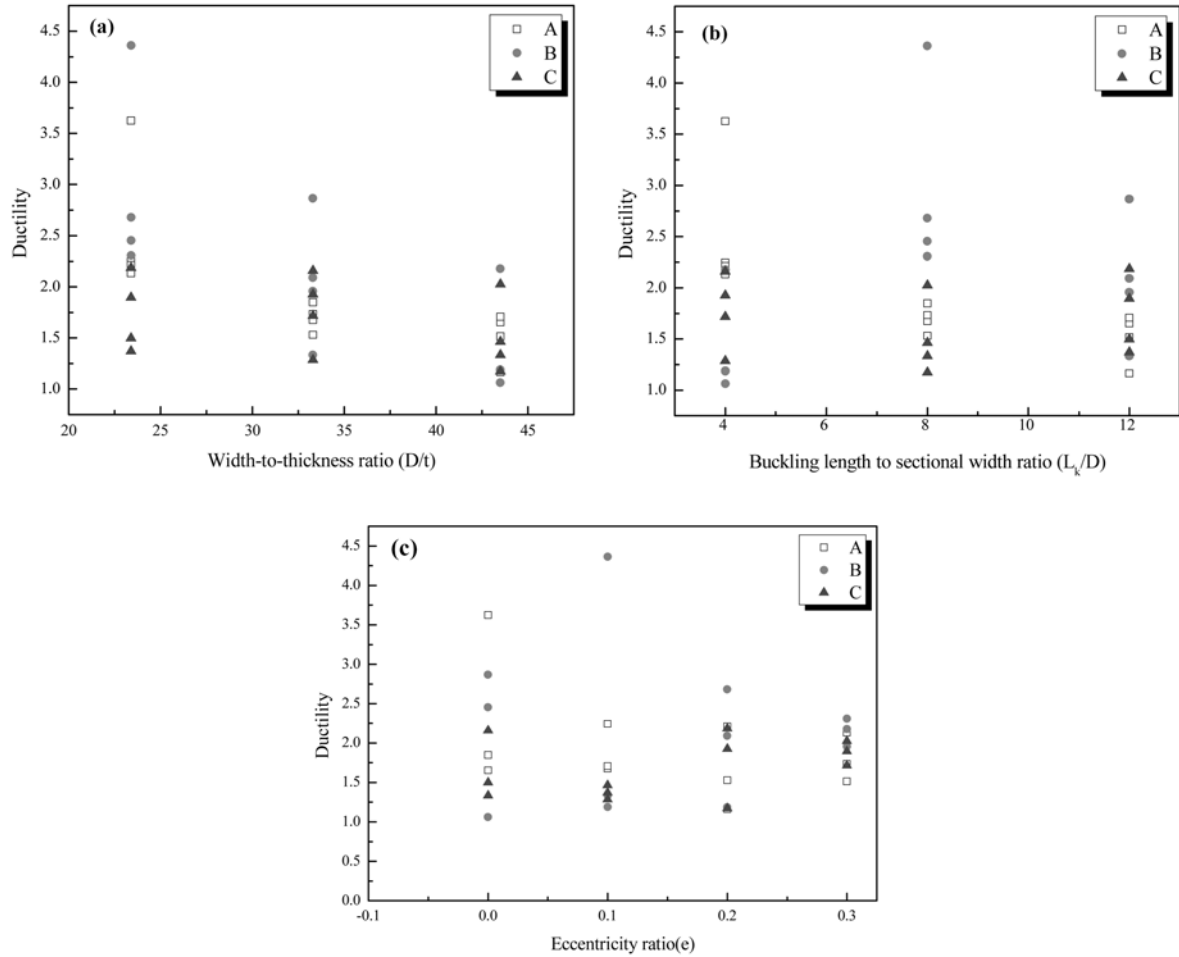


Fig. 4 Influence of (a) width-to-thickness ratio (b) buckling length to sectional width and (c) eccentricity ratio on the displacement ductility ( $\Delta$ )

The design compressive strength for axially loaded filled composite columns shall be determined for the limit state of flexural buckling based on column slenderness as follows:

a) When  $P_e \geq 0.44P_0$

$$P_n = P_o [0.658^{(P_o/P_e)}] \quad (2)$$

b) When  $P_e < 0.44P_0$

$$P_n = 0.877P_e \quad (3)$$

Where

$$P_o = A_s F_y + A_{sr} F_{yr} + 0.85 A_c f'_c \quad (4)$$

$$P_e = \pi^2 (EI_{eff}) / (KL)^2 \quad (5)$$

#### 4.2 AIJ-recommendations for design and construction of CFT ( $N_{AIJ}$ )

『Recommendations for Design and Construction of Concrete-Filled Steel Tubular Structures』 (1997, hereinafter “CFT” recommendations) reflects study results on CFT structures from the Architectural Institute of Japan (AIJ). The compressive strength of a column member according to the buckling length-sectional width ratio ( $L_k/D$ ) is generally calculated by (6)-(8) formulas.

$$(L_k/D \leq 4): N_{AIJ} = A_s \cdot F_y + A_c \cdot \sigma_{cr} \cdot f_{cu} \quad (6)$$

$$(4 < L_k/D \leq 12): \{N_{AIJ} = N_{u1} - 0.125(N_{u1} - N_{u2}) \cdot (L_k/D - 4)\} \quad (7)$$

$$(12 < L_k/D): \{N_{AIJ} = {}_sN_u + {}_cN_u\} \quad (8)$$

The ultimate axial capacity of a slender column according to CFT recommendations is calculated by using the following formula, a superimposed strength method, which accumulates the capacity of the slender column steel tube and concrete by considering secondary bending effects.

$$(N_{AIJ} \leq {}_cN_{cu}, M \geq {}_sM_{uo}(1 - {}_cN_{cu}/N_k)), N_{AIJ} = {}_cN_u \quad (9)$$

$$M = {}_cM_u + {}_sM_{uo}(1 - {}_cN_u/N_k) \quad (10)$$

$$(N_{AIJ} \leq {}_cN_{cu}, M < {}_sM_{uo}(1 - {}_cN_{cu}/N_k)), N_{AIJ} = {}_cN_{cu} + {}_sN_u \quad (11)$$

$$M = {}_sM_u(1 - {}_cN_{cu}/N_k) \quad (12)$$

$$N_k = \pi^2(E_c I_c / 5 + E_s I_s) / L_k^2 \quad (13)$$

#### 4.3 AIJ-SRC standards ( $N_m$ )

The Standards for Structural Calculation of Steel Reinforced Concrete Structures (AIJ 1987) were used to modify the existing formula. Compared to CFT recommendations, there are no fundamental modifications, but this modification is for the ultimate axial capacity of a concrete column for slender columns (Condition:  ${}_cN_{cu} \rightarrow N_m \leq 0.9 \rightarrow {}_cN_{cu}$ ,  $N_m > 0.9 {}_cN_{cu}$ ).

$${}_cN_{cu} = {}_c\sigma_{cr} \cdot A_c, {}_c\lambda_1 \leq 1.0, {}_c\lambda_1 = \frac{\lambda \sqrt{\varepsilon_u}}{\pi} \quad (14)$$

$$\frac{{}_c\sigma_{cr}}{f_{cu}} = \frac{2}{1 + \sqrt{{}_c\lambda_1^4 + 1}} \quad (15)$$

$${}_c\lambda_1 \geq 1.0, \frac{{}_c\sigma_{cr}}{f_{cu}} = 2(\sqrt{2} - 1)\{a_c(1 - {}_c\lambda_1)\} \quad (16)$$

Where  $f_{cu}$  is the compressive strength of concrete and  $a_c$  is the factor dependent on the compressive strength of concrete, the values are 0.70 ( $f_{cu} = 23.5$  MPa), 0.80 ( $f_{cu} = 35.3$  MPa), 0.86 ( $f_{cu} = 47.0$  MPa), 0.92 ( $f_{cu} = 58.8$  MPa) and 1.02 ( $f_{cu} = 94.08$  MPa). Also, where  ${}_c\sigma_{cr}$  is the buckling stress of concrete and  ${}_c\lambda_1$  is the slenderness ratio of concrete column, respectively, the  $\varepsilon_u$  represents strain for the compressive strength of concrete in the following formula;  $\varepsilon_u = 0.93(f_{cu})^{1/4} \times 10^3$ .

#### 4.4 Takanori Sato's proposal ( $N_T$ )

This proposal for a simplified and unified design method for concrete-filled steel tubes in short columns to slender columns suggested by Sato (1999), focused on practical use (Dec. 1999). Also, it was based on the sectional capacity of short columns; the proposal definitely completes a generalized superimposed capacity concept. Generally, the ultimate state of the member is determined by its role and function. The first function of a column is to support vertical load. Fig. 5 illustrates by an eccentric compression test the typical  $N$ - $M$  relation of the plastic hinge in the center.

##### 4.4.1 Column curve

The central compressive strength of a column is supported by pins at both ends; that is, buckling capacity ( $N_{cr}$ ) decreases according to the buckling length-sectional width ratio ( $L_k/D$ ). The column curve shows the relation between the reduction rates ( ${}_cR_{cr}$ ,  ${}_sR_{cr}$ ) of buckling capacity and buckling length-sectional width ratio ( $L_k/D$ ). The column curve for CFT column simply accumulates the curve for the buckling capacity of the steel tube cited from plasticity design standards for steel structures (AIJ 1975). A concrete parabola model from CFT recommendations (AIJ 1997) is shown by the following formula (Lee *et al.* 1998).

$$N_{cr} = A_c \cdot f_{cu} \cdot {}_cR_{cr} + A_s \cdot F_y \cdot {}_sR_{cr} \tag{17}$$

Where  $N_{cr}$  is the buckling capacity of CFT column, the sectional area of concrete ( $A_c$ ) and that of the steel tube ( $A_s$ ),  $f_{cu}$ ,  $F_y$  represent the compressive strength of the concrete and the yield strength of the steel tube, respectively.  ${}_cR_{cr}$  and  ${}_sR_{cr}$  represent the reduction rate of the concrete and the steel tube, respectively. For a range of  $L_k/cD \leq 10$  of the concrete column,  $R_{cr} = 1$  is applied. For  $L_k/sD \leq 9$  of steel tube,  $R_{cr} = 1$  is applied and for other ranges, a bi-linear formula was proposed to reduce as (18)-(19) formulas.

$${}_cR_{cr} = \frac{{}_c\sigma_{cr}}{f_{cu}} = \frac{50 - \frac{L_k}{cD}}{40}, \quad (10 < L_k/cD < 30) \tag{18}$$

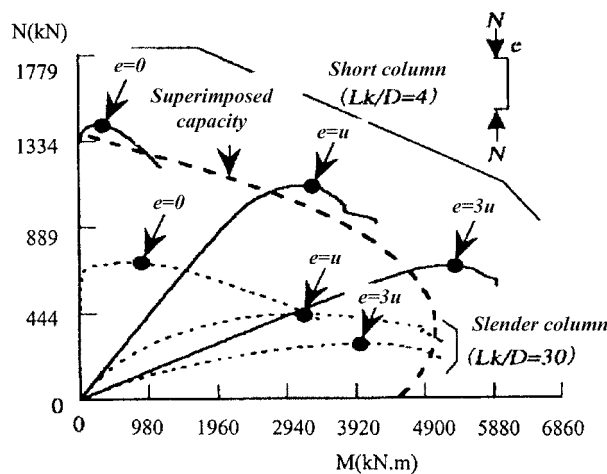


Fig. 5  $N$ - $M$  relationship at column mid-height by eccentric load

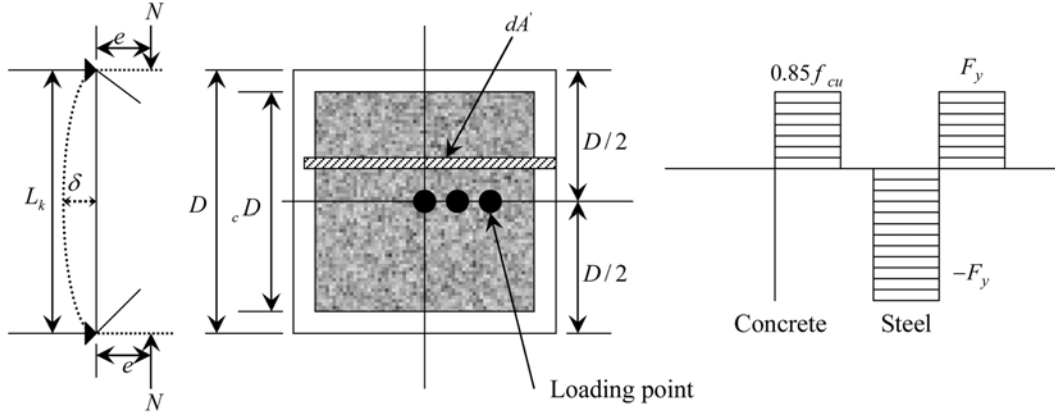


Fig. 6 Load condition and stress distribution of cross section

$${}_sR_{cr} = \frac{{}_s\sigma_{cr}}{f_{cu}} = \frac{90 - \frac{F_y}{150} \frac{L_k}{sD}}{81 - \frac{F_y}{150}}, \quad (9 < L_k / sD < 30) \quad (19)$$

#### 4.4.2 Sectional capacity

The sectional capacity ( $M_{ucr}$ ,  $N_{ucr}$ ) of the plastic hinge without confined effect is represented in Fig. 7. It's said to be a function of buckling length-sectional width ratio ( $L_k / D$ ) with continuation from a short column to a slender one. Therefore, the sectional capacity of a CFT column is between maximum yield capacity and total plastic moment ( $M_u$ )-axial capacity ( $N_u$ ) according to buckling length-sectional width ratio ( $L_k / D$ ). The yield stress at maximum yield capacity is the yield strength ( $F_y$ ) of the steel tube and 85% ( $0.85f_{cu}$ ) of its compressive strength amounting to the critical strength for concrete, respectively, as shown in Fig. 6.

Therefore, Sato (1999) proposes a sectional capacity ( $M_{ucr}$ ,  $N_{ucr}$ ) powering reduction ratio by the column curve in the same moment ( $M$ )-ultimate axial load capacity ( $N$ ) of the existing design (AIJ 1997).

$$M_{ucr} = R_{cr}^3 \cdot M_u + (1 - R_{cr}^3) \cdot M_{AS} \quad (20)$$

$$N_{ucr} = \{R_{cr}^3 \cdot N_u + (1 - R_{cr}^3) \cdot N_{AS}\} \cdot R_{cr} \quad (21)$$

### 4.5 Comparison of test results with current codes

#### 4.5.1 Influences of buckling length-sectional width ratio

The moment ( $M$ )-ultimate axial load capacity ( $N$ ) ultimate for a member with a high  $L_k / D$  ratio is commonly determined by bending moment or buckling, in cases where only concentrically axial load is applied on CFT member. The capacity of members with a low  $L_k / D$  ratio is related to the local buckling of steel, crushing of concrete and a confining effect of steel on the dilatancy of crushed concrete. One of the major factors that effect of the behavior is the buckling length to sectional width ratio ( $L_k / D$ ) for a compression test of a column.

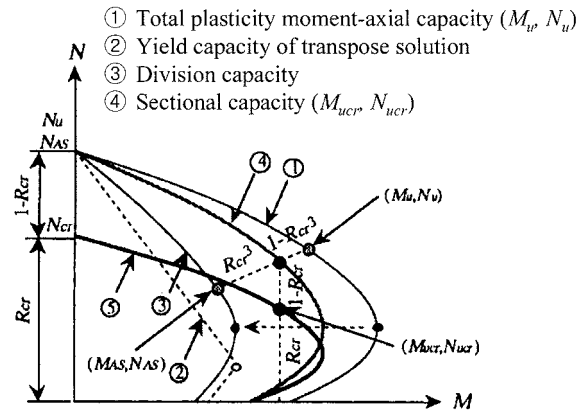


Fig. 7 Sectional capacity by buckling length-width ratio

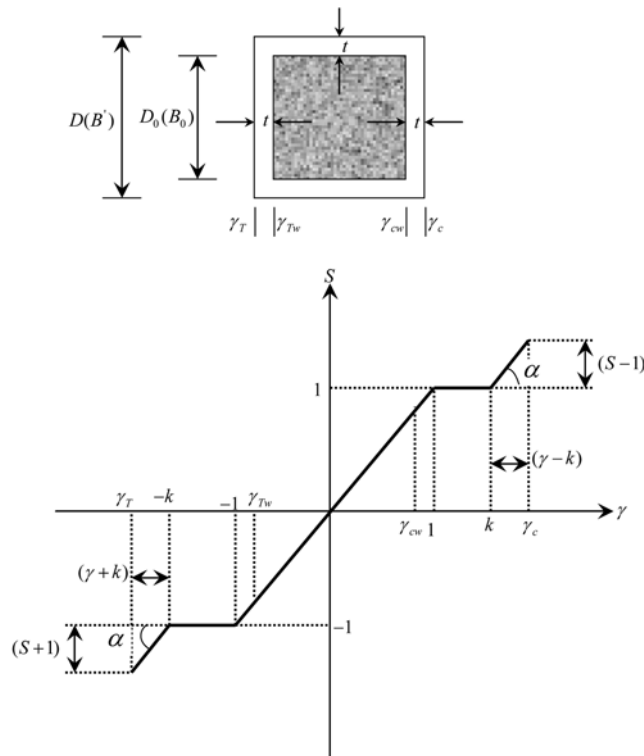


Fig. 8 Stress-strain relation including strain hardening of steel

The experimental capacity-calculated capacity ( $N_{exp}/N_{cal}$ ) decreases with an increase in the buckling length to sectional width ratio ( $L_k/D$ ). This trend was proved by the existing research of Saadeghvaziri (1999), Tomii *et al.* (1977). However, the paper by Saadeghvaziri (1999) says that the range of the width-thickness ratio ( $D/t = 20$ ) for a square short steel column is  $L_k/D < 7$  which is a little different from that of the AIJ-CFT recommendations (1997).  $L_k/D$  results of A, B and C-type specimens of  $N_T$  show low values with a contrary trend for those of  $N_L$ , as shown in Fig. 11. As in Fig. 11, B type specimens, between 0.818 and 1.312 in (a), between 0.747 and 1.182 in (b) and between 0.633 and 1.182 in (c)

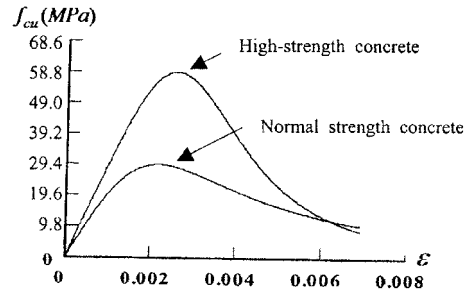


Fig. 9 Concrete stress-strain model under cyclic load: Popovics

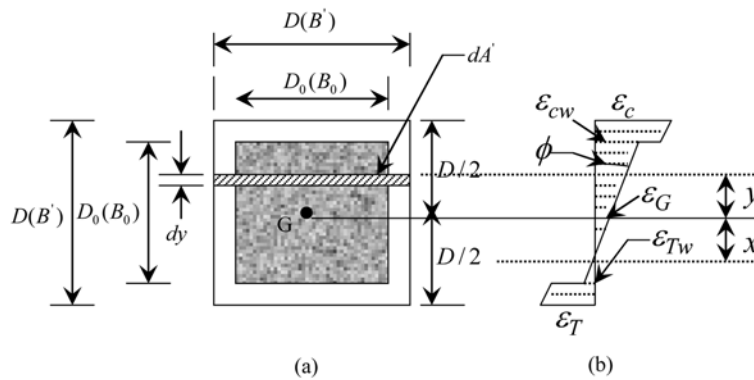


Fig. 10 Square steel tube and assumption of stress distribution

indicate that the  $L_k/D$  increases according to the rise in non-dimensional width-thickness ratio ( $\bar{a} = \sqrt{F_y/E_s} \times D/t$ ) are underestimated with the experimental capacity-calculated capacity ( $N_{exp}/N_{cal}$ ). It appears notable for A, B and C type specimens with a non-dimensional width-thickness ratio  $\bar{a} = 1.842$ . Table 4 shows the results of the ultimate axial load ( $N$ ) capacity in various codes based on the buckling length to sectional width ratio ( $L_k/D$ ).

#### 4.5.2 Influence of high-strength concrete

AISC-LRFD (2005) is based on the bilinear interaction formula for calculating strength interaction between ultimate axial load ( $N$ ) and moment ( $M$ ). It is the same type as for the steel-frame column. However, in the case of Japan's articles 3.2 (AIJ 1997) to 3.4 (Sato 1999), the concept of general cumulative strength as a continuous concept from short column to slender column for strength has been completed. Generally the AISC-LRFD (2005) design gets more precise with i) an increase in the sectional area of the structural steel, ii) a decrease in the concrete's strength, or iii) a reduction in concrete coherence under bending moment ( $M$ ) behavior. However, AISC-LRFD (2005) is difficult to apply for either high-strength concrete or members under high axial load. It is noted that higher strength concrete materials may be used for stiffness calculations but may not be relied upon for strength calculations unless justified by testing or analysis. For example, the Fly-ash (B) for concrete model ( $L_k/D = 12$ ) of  $N_T$  (Sato 1999) shows a 29% reduction compared to other specimens as shown in Fig. 12. Therefore, a modified compressive strength formula is considered an improvement, as it is a better method for calculating capacity  $N-M$  without damaging the effectiveness of the composite

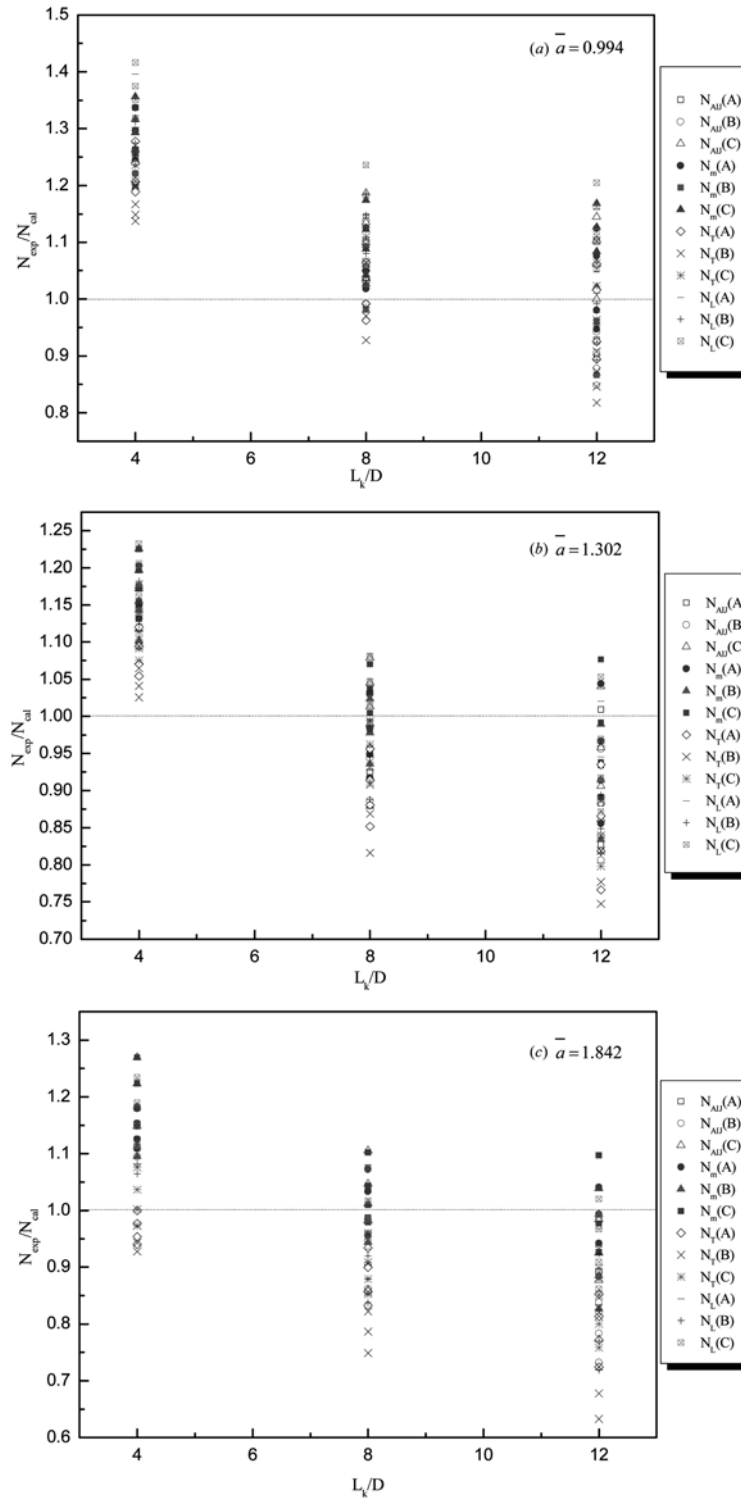


Fig. 11 Non-dimensional  $L_k/D$  vs  $N_{exp}/N_{cal}$

Table 3 Constants  $\alpha$ ,  $\beta$ ,  $\eta$ ,  $\omega$  of Popovics

Strength of mixed design (MPa)	$\alpha$	$\beta$	$\eta$	$\omega$
58.8	$-10.2 \times 10^{-4}$	$2.36 \times 10^{-1}$	$-5.112 \times 10^{-4}$	1.892

Table 4 Test results of columns ( $N$ - $M$ )

$D/t$	$e$	$L_k/D$	$L_k$	$N_{AIJ}$ (kN)	$N_M$ (kN)	$N_T$ (kN)	$N_L$ (kN)	$N_{exp}$ (kN)		
								A	B	C
23.4	0.0	4	29.1	500.0	500.0	523.1	478.8	668.3	628.1	678.1
	0.1							648.3	610.4	658.2
	0.2							631.3	600.8	646.5
	0.3							622.0	595.0	631.5
	0.0	8	58.2	488.4	493.7	522.2	469.0	556.0	555.8	579.5
	0.1							539.3	538.1	554.3
	0.2							518.0	506.8	537.2
	0.3							502.6	484.5	514.7
	0.0	12	87.3	477.7	467.9	495.5	453.8	526.1	450.0	546.7
	0.1							503.3	432.6	527.1
	0.2							458.7	419.2	507.2
	0.3							443.1	405.3	477.6
33.3	0.0	4	39.3	772.2	772.2	829.1	767.9	928.7	907.7	946.1
	0.1							907.4	882.7	923.9
	0.2							887.6	863.0	904.7
	0.3							874.0	850.3	891.8
	0.0	8	78.6	757.0	763.3	822.0	755.4	786.0	781.2	816.8
	0.1							751.3	746.4	791.1
	0.2							724.0	714.3	766.8
	0.3							700.2	670.9	749.2
	0.0	12	117.9	742.8	717.9	801.5	734.1	749.3	710.2	772.9
	0.1							693.9	656.3	711.7
	0.2							655.9	622.9	673.2
	0.3							614.1	599.0	639.8
43.5	0.0	4	39.7	657.4	657.4	775.7	676.0	775.6	777.3	834.4
	0.1							758.0	755.2	804.0
	0.2							739.8	731.5	777.3
	0.3							729.2	719.8	754.7
	0.0	8	79.4	647.6	649.4	745.5	666.2	696.2	638.3	715.8
	0.1							670.9	612.8	677.5
	0.2							639.3	586.2	655.5
	0.3							620.8	558.2	635.7
	0.0	12	119.1	637.8	604.0	737.5	649.3	628.7	600.0	662.4
	0.1							599.9	534.6	627.7
	0.2							569.2	499.8	590.1
	0.3							534.0	466.9	559.5

column. It is a validation of the design within AISC-LRFD (2005) model and with a bilinear type maintained to include nominal compressive strength ( $P_n$ ), strength at the balancing point for the effect above  $f_c = 58.8$  MPa.

A specimen with  $L_k/D = 4$  and  $D/t = 23.4$  of  $N_{AIJ}$  (1997) approaches sectional capacity ( $M_{ucr}$ ,  $N_{ucr}$ ),

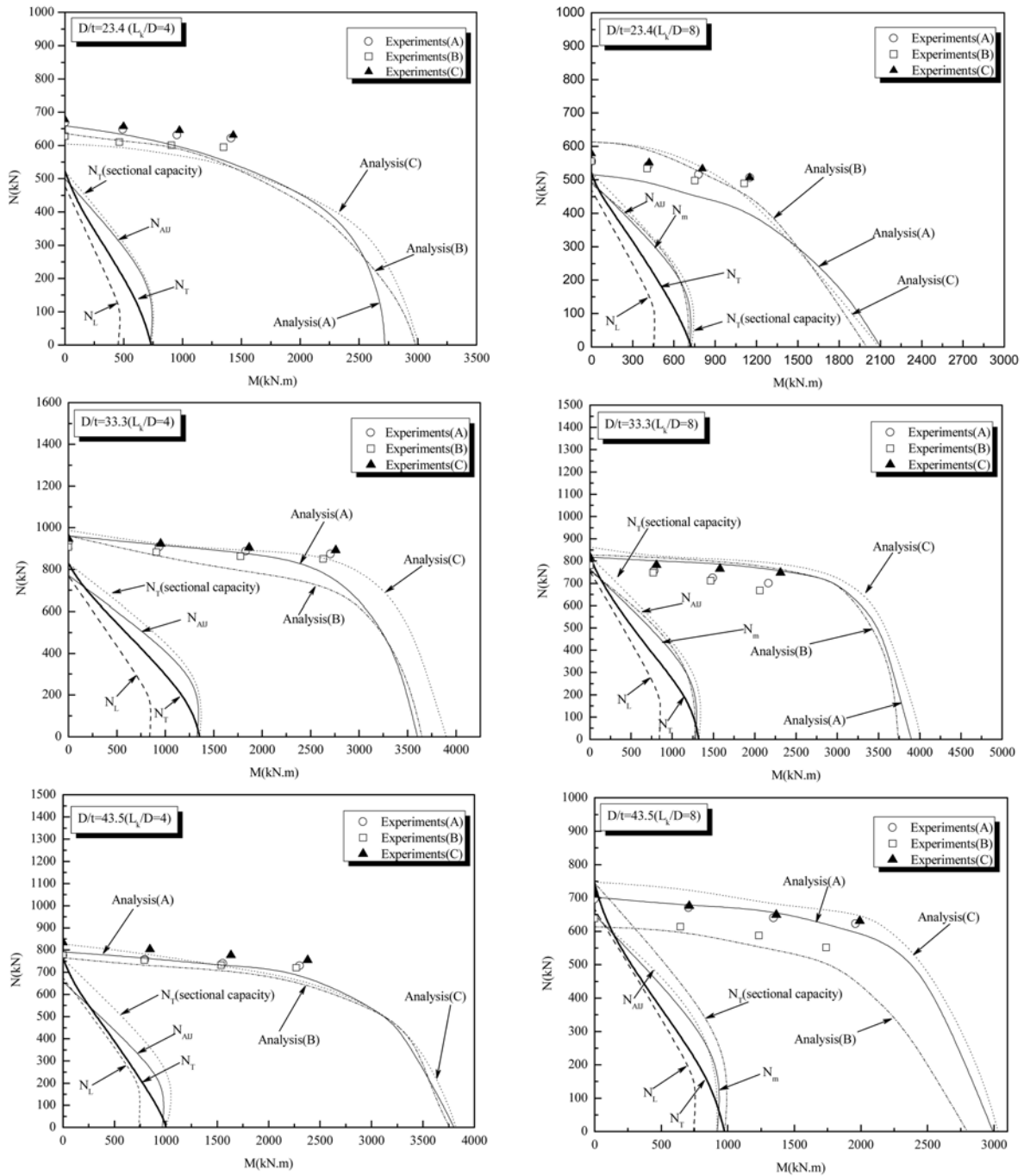


Fig. 12 Comparison of capacity ( $N-M$ )

and with an increase in width-thickness ratio ( $D/t$ ),  $N_{AU}$  (1997) tends to decline to a member capacity of  $N_T$  (Sato 1999). Mostly, a specimen with  $D/t = 33.3$  shows the higher values of ultimate axial load ( $N$ ) with from 1.78 to 1.81 differences for the  $D/t = 23.4$  and from 1.35 to 1.4 for the  $D/t = 43.5$ , respectively.

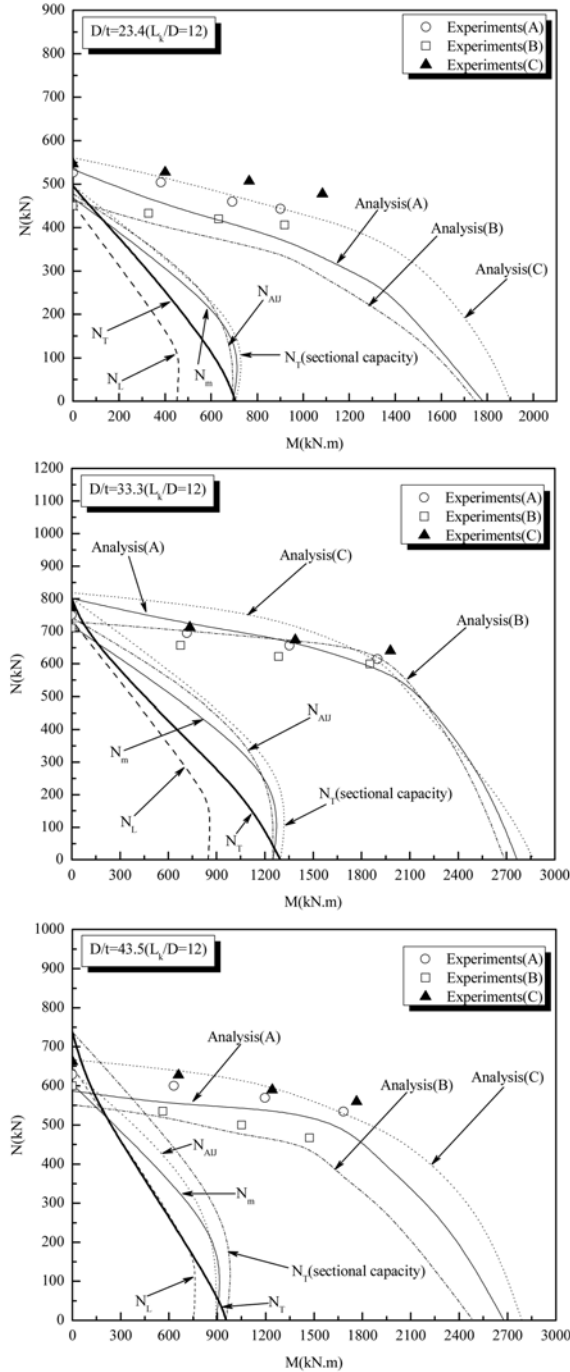


Fig. 12 (Continued) Comparison of capacity ( $N$ - $M$ )

Overall, it shows  $N_L < N_{AIJ}$ ,  $N_m < N_T$  for capacity, especially for  $N_{AIJ}$  and  $N_m$  (AIJ 1987):  $N_{AIJ}$  shows a greater value for initial ultimate axial load ( $N$ ). It is found that for ultimate axial load ( $N$ ),  $N_m$  (AIJ 1987) tends to approach that of a member capacity. This is due to 0.92 being the value for the compressive

strength of filled concrete at  $f_c = 58.8$  MPa and a conversion of concrete strain from 0.52 to 0.93 in compressive strength. In  $N_{AIJ}$  (AIJ 1997), 0.9 times of a coefficient for the compressive strength ( $_cN_{cu}$ ) of a slender column is applied.

A specimen of  $N_L$  tends to approach that of a  $N_T$  capacity with an increase in width-thickness ratio. It is noted that an ultimate axial load cross-section model is used to determine the section capacity. This model is similar to that used in previous LRFD Specifications. The major difference is that the full strength of the reinforcing steel and concrete are accounted for rather than the 70 percent that was used in those previous specifications. In addition, these provisions give the strength of the composite section as a force, while the previous approach had converted that force to an equivalent stress. Since the reinforcing steel and concrete had been arbitrarily discounted, the previous provisions did not accurately predict strength for columns with a low percentage of steel.

#### 4.5.3 Investigations in the current codes

There are limitations in the compressive strength of concrete for CFT. In the case of AISC-LRFD (2005), the range is limited:  $21 \text{ MPa} \leq f_c \leq 70 \text{ MPa}$  and the Architectural Institute of Korea (AIK 2004) has set 49 MPa for the maximum compressive strength of concrete. In addition, AISC-LRFD (2005) restricts the nominal yield strength of steel to about 525 MPa considering a concrete crushing at 0.003 of strain. That is, for net axial load, the yield of steel before concrete crushing prevents the brittle failure of the concrete.

However, many experiments carried out in Japan have proven the effectiveness of high-strength steel (see AIJ 1997, Saito *et al.* 1989). That is due to the confined effect of steel delaying the brittle failure of concrete. In this situation, AIK (2004) sets forth 392 MPa of maximum nominal yield stress for high-strength reinforcing bar and steel tube. AISC-LRFD (2005) stipulates that the sectional area of steel be more than 1% of that of the filled steel tube; however, in AIK (2004) the sectional area of the steel frame in a composite column is more than 3% of the total area. By contrast, Japan requires total 0.8% for steel and reinforcing bar ratio. In previous AISC-LRFD, which requires the greatest sectional area, when the sectional area of steel is less than 4% of the total area, subjects must be designed according to ACI standards.

Therefore, in this specification, the use of composite columns is extended from the previous minimum steel ratio of 4 percent (area of steel shape divided by the gross area of the member) down to columns with a minimum of 1 percent. This is a direct result of using an ultimate strength cross-sectional approach, and removes the previous discontinuities in design that occurred as the steel ratio decreased below 4 percent.

In the case of the Euro code 4 (1994), Design of Steel Structures, the ultimate axial load ( $N$ ) of steel is required to be more than 20% of the total sectional capacity. If this is applied to both the practical material strength and the column section, this value is approximately equal to 2% of the steel ratio.

The low strength concrete is not recommended to select concrete for CFT, when a high-strength steel tube is used to prevent prior crushing of concrete in an ultimate state. Lee *et al.* (2000, 1998) states that concrete between 20.58 and 39.2 MPa showed a desquamation of concrete from the inner surface of the steel due to the shrinkage of the concrete. In the case of high-strength concrete with 58.8 MPa, the preceding dilatancy of the steel tube prevents the expansion of the concrete and crushing.

## 5. HCFT analytical model

The results from the experimental investigations and the current code provisions provide significant insight into the behavior of HCFT columns. In addition to a basic presumption regarding the composition of

the material, the hypotheses are applied to analyze the axial load ( $N$ )-moment ( $M$ )-curvature ( $\phi$ ) relation: i) to maintain cross-section, ii) to maintain plane, iii) to ignore the tensile stress of the concrete for HCFT, iv) to assume that the stress-strain of concrete for HCFT is equal according to the position of the section, v) to have tri-linear type considering perfect elasto-plastic stress-strain by the combination of compressing the steel tube and strain hardening it by tension. The starting point of strain hardening is  $k$  ( $= \varepsilon_{st}/\varepsilon_y, \varepsilon_{ST}$ ), and the slope of strain hardening curves is  $a$  ( $= E_{ST}/E, E_{ST}$ : tangent modulus of strain hardening curve); both of which are assumed to be symmetric in compression and tension sides, as shown in Fig. 8.

This study has both axial capacity and the non-dimensional width-thickness ratio ( $\bar{a}$ ) as major variables and the analysis of the axial load ( $N$ )-moment ( $M$ )-curvature ( $\phi$ ) relation provides transformation performance on the strain hardening of the column.

### 5.1 Steel

The tangent modulus of the square steel tube section on the compression side ( $r_c$ ) and tension side ( $r_T$ ) is set as  $E = 1.0$ . The stress ( $S$ )-strain ( $r$ ) curve of the steel in Fig. 8 consists of 2 straight lines with a definite yield point, a length of plastic flowing range,  $k$  ( $= \varepsilon_{st}/\varepsilon_y, \varepsilon_{st}$ ; strain at the starting point of strain hardening) and a straight line with a tangent modulus of the strain hardening curve,  $\alpha$  ( $= E_{st}/E, E_{st}$ ; second tangent modulus at the starting point of strain hardening) as a slope. The following formulas are given for each range with the symmetric section of the  $S$ - $r$  curve.

$$k \leq r: \alpha = E_{st}/E = E_{ST} = \frac{S-1}{r-k}; S = \alpha(r-k) + 1, \quad -k < r < -1; S = -1 \quad (22)$$

$$-k < r: \alpha = E_{ST} = \frac{S+1}{r+k}; S = \alpha(r+k) - 1, \quad -1 \leq r < 1; S = r, \quad 1 \leq r < k; S = 1 \quad (23)$$

### 5.2 Concrete

Generally, the stress-strain of material in the elastic range can be explained by Hooke's law with  $\sigma = E \cdot \varepsilon$ . However, it can be seen that  $\sigma = A'(\varepsilon) \cdot E \cdot \varepsilon$  because the concrete's stress-strain interaction relative to plastic range shows a decrease in the slope of the tangent when it passes through the elastic range, approximately 1/3 of the maximum compressive stress and enters plastic range to the maximum strength. This paper uses Popovics's (1973) proposal, a relatively precise analytic model for stress-strain in concrete, and the models of materials used for the analysis are listed in Fig. 8.

$$\sigma = E \cdot \varepsilon \frac{n-1}{n-1 + (\varepsilon/\varepsilon_0)^n} \quad (24)$$

In the above formula,  $(n-1)/\{n-1+(\varepsilon/\varepsilon_0)^n\}$  is applicable to  $A'(\varepsilon)$  representing its relation to a slope of tangent. This slope differs between normal concrete and high-strength concrete. The following formulas are used to determine the relation between the optimal experimental constant ( $n$ ) through hysteretic behavior experiments by using 28-day concrete with 58.8 MPa of mixing strength and  $f_{cu}$ , and  $\varepsilon_0$  and  $f_{cu}$ , respectively.

$$\varepsilon_0 = \alpha \cdot f_{cu} + \beta, \quad n = \eta \cdot f_{cu} + \omega \quad (25)$$

### 5.3 Modeling of axial load – bending moment – curvature analysis ( $N-M-\phi$ )

The following is the basic formula for elasto-plastic bending moment-curvature ( $M-\phi$ ) based on the experimental results and cross-sectional stress distribution presumed in Fig. 10, when the symmetric sectional curvature  $\phi$  is  $\gamma_c > 0, \gamma_T < 0$  :

$$\phi = \frac{\varepsilon_c + \varepsilon_{cw} - \varepsilon_T - \varepsilon_{Tw}}{D} = \frac{\gamma_c + \gamma_{cw} - \gamma_T - \gamma_{Tw}}{2} \left( \frac{\varepsilon_x}{D/2} \right)$$

Also, yield curvature  $\phi_x$ , as,  $\phi_x = \frac{\varepsilon_x}{D/2}$ , curvature ratio  $\varphi$ :

$$\varphi = \phi / \phi_x = \frac{\gamma_c + \gamma_{cw} - \gamma_T - \gamma_{Tw}}{2} \quad (26)$$

in which,

$$\begin{aligned} \{ \gamma_c = \varepsilon_c / \varepsilon_x, \gamma_{cw} = \varepsilon_{cw} / \varepsilon_x \} &> 0 \\ \{ \gamma_T = \varepsilon_T / \varepsilon_x, \gamma_{Tw} = \varepsilon_{Tw} / \varepsilon_x \} &< 0 \end{aligned}$$

The distance ( $x$ ) from a section center in coordinate axis is expressed by

$$x = \frac{\gamma}{\gamma_c - \gamma_G} \times \frac{D}{2} = \xi \times \frac{D}{2} \quad (27)$$

$$\xi = \frac{\gamma}{\gamma_c - \gamma_G}, \quad \gamma_G = \frac{\gamma_c + \gamma_{cw} + \gamma_T + \gamma_{Tw}}{4}, \quad (\gamma_c, \gamma_{cw}) > 0, \quad (\gamma_T, \gamma_{Tw}) < 0 \quad (28)$$

where  $\gamma_G$  is the equilibrium strain ratio,  $\gamma$  is the strain ratio on a distance ( $y$ ) at the centroid of section. To evaluate the ultimate axial load capacity ( $N$ ) of CFT columns, the ultimate axial load capacity ( $N$ ) is defined as

$$N = \sigma_0 \times A' = \sigma_x B' \frac{D}{2} \int_{\gamma_T \gamma_c - \gamma_G}^{\gamma_c} \frac{S b' d_e}{\gamma_c - \gamma_G} \quad (29)$$

where  $\sigma_0$  is the existence stress from the centroid to distance ( $y$ ),  $B'$  is the maximum of the sectional width and  $B_0$  is the sectional width of the temporary,  $S_0$  is the axial load capacity ratio of the existence.

$$\frac{B' - B_0}{B_0} = b', \quad y = \frac{D}{2} \xi, \quad S_0 = \frac{\sigma_0}{\sigma_x} \quad (30)$$

$$-\frac{D_0}{2} < y < \frac{D_0}{2}, \quad -1 < \xi < 1, \quad d\xi = \frac{d_e}{\gamma_c - \gamma_G} \quad (31)$$

The cross sectional area ( $A'$ ) and a coefficient of the concrete filled steel tube shape ( $\alpha', \beta'$ ) is denoted as

$$A' = -4t^2 + 2t(D + B') \quad (32)$$

$$\alpha' = \frac{1}{1 - (1 - 2t)^2}, \quad \beta' = \frac{1}{1 - (1 - 2t)^4} \quad (33)$$

$$\sigma_x \cdot B' \cdot D = N_x = \frac{B'D}{A'} \cdot \sigma_x \cdot A' = \alpha' \cdot \sigma_x \cdot A' = \alpha' N_x \quad (34)$$

The ultimate axial load capacity ( $N$ ) can be proposed as formula (35), and the equilibrium of concentric axial load and sectional bending moment ( $M$ ) can be proposed as formula (36) from the equilibrium condition.

$$N = N_x \cdot \frac{1}{2(\gamma_c - \gamma_G)} \int_{\gamma_T}^{\gamma_c} S b' d_e = \alpha' \cdot \frac{N_x}{2(\gamma_c - \gamma_G)} \int_{\gamma_T}^{\gamma_c} S b' d_e \quad (35)$$

$$M = \int_{-1}^1 \frac{\sigma D^2 (B' - B_0)}{4} \xi d\xi = \frac{\sigma_x B' D^2}{4(\gamma_c - \gamma_G)^2} \int_{\gamma_T}^{\gamma_c} S b' (\gamma_c - \gamma_G) d_e \quad (36)$$

The yield moment  $M_x$  can be expressed as follows:

$$M_x = \sigma_x \cdot Z, \quad M_0 = \frac{\sigma_x \cdot B' \cdot D^2}{6}, \quad \beta' = \frac{B' \cdot D^2}{6Z} \quad (37)$$

$$m = M/M_x = M\beta'/M_0 \quad (38)$$

in which  $m$  is the yield ratio due to bending moment ( $M$ ) effect, respectively.

#### 5.4 Axial load-bending moment-curvature analysis ( $N$ - $M$ - $\phi$ )

The numerical analysis interaction curves including of concrete admixture (Zeolite, Fly-ash and Silica-fume) for CFT were compared with the interaction curves of the experiments result are shown in Fig. 12. Generally, the numerical results show good agreement with the experimental data. From the Fig. 12, it is observed that the value of axial load-bending moment ( $N$ - $M$ ) capacity for  $L_k/D = 33.3$  is higher than that for the  $D/t = 23.4$ ,  $D/t = 43.5$ . Also, Fig. 12 indicates that the  $L_k/D = 23.4$  ( $L_k/D = 8$ ) underestimates the ultimate axial load capacity ( $N$ ) of the Analysis (A). The analysis-predicted axial load-bending moment ( $N$ - $M$ ) capacity is significantly accurate and conservative for specimens with  $L_k/D = 4$ . The  $D/t = 33.3$  ( $L_k/D = 4$ ) shows the axial load-bending moment ( $N$ - $M$ ) capacity of the Analysis (c) result at the value of Experiments (c) result very close. As a result, the capacity degradation for columns with an Analysis (A) would be higher than that for column with an Analysis (B) but lower than that for columns with an Analysis (C).

Fig. 13 curves bending moment ( $M$ ) versus curvature ( $\phi$ ) with a non-dimensional width-to-thickness ratio ( $\bar{a}$ ). Fig. 13 shows that an increase in non-dimensional width-to-thickness ratio ( $\bar{a}$ ) tends to rise bending moment ( $M$ ) value. From the figure, regardless of width-to-thickness ( $D/t$ ) ratio change, no difference is found in the initial stiffness. For a steel tube with a curvature ( $\phi$ ) in the corner, this tendency is caused more by the bending confinement effect of the corner with the curvature ( $\phi$ ) than by

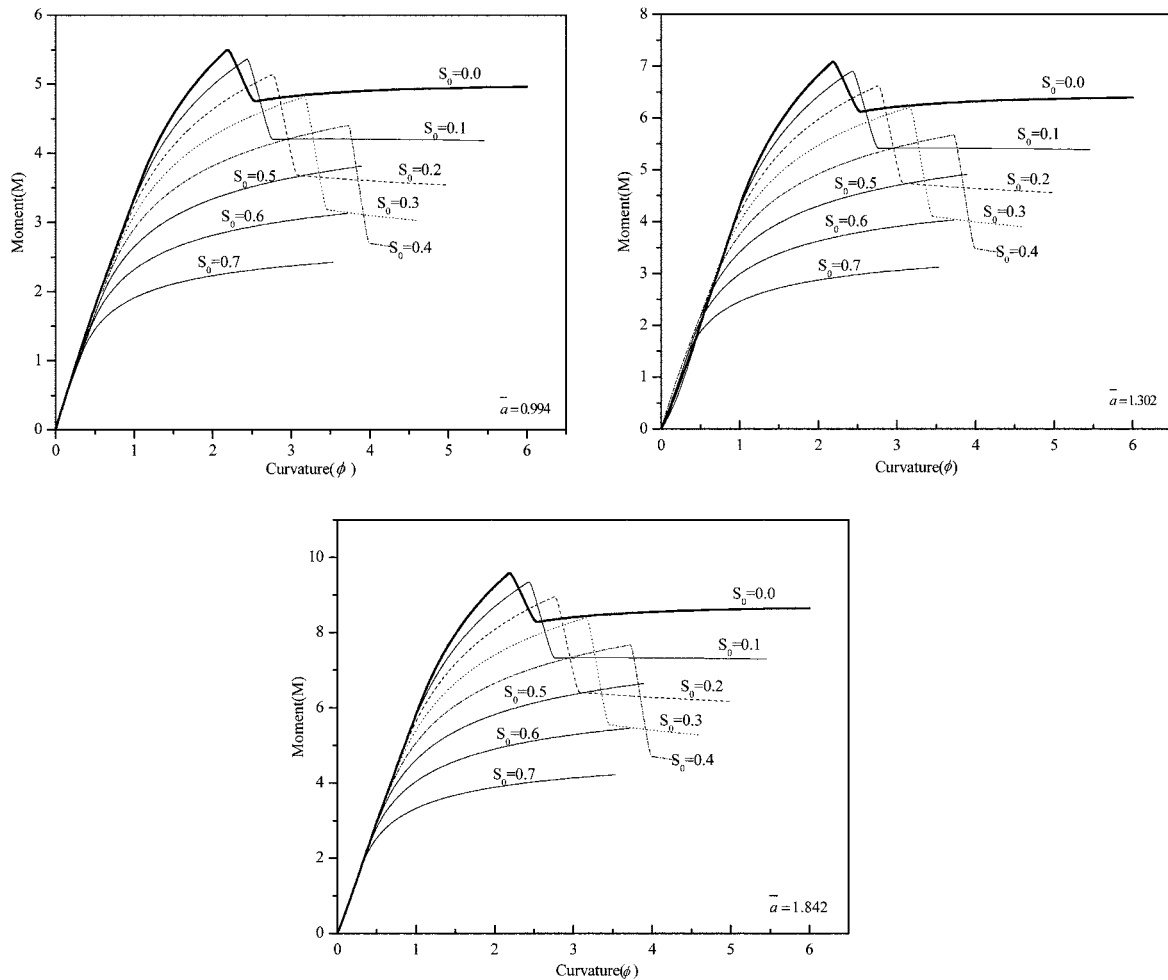


Fig. 13 Analytical result of moment ( $M$ ) - curvature ( $\phi$ )

defining the width of the plate as an outer dimension and decreasing the sectional area. The curvature ( $\phi$ ) increases as the bending moment ( $M$ ) in the strain hardening range decreases through the elasto-plastic range, as shown in Fig. 13. The capacity of HCFT columns decreases significantly with an increase in the axial load capacity ratio ( $S_0$ ).

Fig. 14 compares experimental results with analytical results in bending moment ( $M$ ) versus curvature ( $\phi$ ) according to width-thickness ( $D/t$ ) ratio change. It is shown from the comparisons that the increase in bending moment ( $M$ ) capacity and initial stiffness was most significant in members with  $D/t$  ratios equaling 43.5. Analytic results agree with experimental results in the initial stiffness. However, analytic results and experimental results slightly disagree after the peak of moment-curvature ( $M$ - $\phi$ ). From the figure, it can be concluded that as long as high-strength steel tubes and filled with high-strength concretes are used, the influence of  $D/t$  ratio is significant. Also, it can be concluded that moment ( $M$ ) increases with an increase in width-to-thickness ratio ( $D/t$ ).

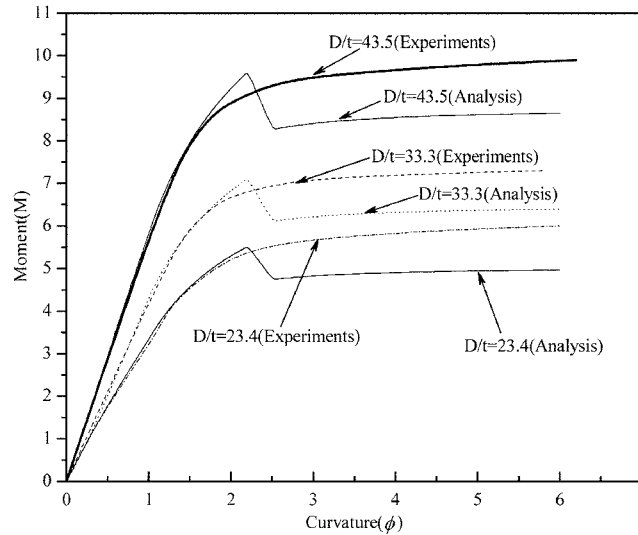


Fig. 14 Comparison of experimental and analysis results by change in  $D/t$  ratios

## 6. Conclusions

This paper described a series of tests on high-strength concrete CFT columns under eccentric loads. Influence of width-to-thickness ( $D/t$ ) ratio and buckling length-sectional width ( $L_k/D$ ) ratio, eccentricity ( $e$ ) ratio on the behavior of HCFT columns was analyzed. The predicted column ultimate axial load capacity using four different design methods,  $N_L$  (AISC-LRFD 2005),  $N_{AJJ}$  (1997),  $N_m$  (1987) and  $N_T$  (Sato 1999) were compared with test results. From these studies, the following conclusions can be inferred:

1) The ductility ( $\Delta$ ) of high-strength CFT columns decrease significantly with an increase in the width-to-thickness ( $D/t$ ) ratio of the steel tube. The C-specimen of buckling length-sectional width ( $L_k/D$ ) ratio and eccentricity ratio ( $e$ ) does not seem to have a significant influence on the  $\Delta$ . The eccentricity ratio ( $e$ ) of the specimen does seem to have a small influence on the  $\Delta$ .

2) The axial load capacity ( $N_{exp}/N_{cal}$ ) of HCFT columns decreases with an increase in the buckling length-sectional width ( $L_k/D$ ) ratio or the width-to-thickness ( $D/t$ ) ratio of the steel tube. Buckling length to sectional width ratio ( $L_k/D$ ) results of A, B and C type specimens of  $N_T$  show lower values than the other standard with a contrary trend for those by  $N_L$ . The axial load capacity ( $N_{exp}/N_{cal}$ ) of Fly-ash (B) type specimen decreases more significantly with an increase in buckling length-sectional width ( $L_k/D$ ) ratio. At larger ( $L_k/D$ ), the yield strength of the steel ( $F_y$ ) and width-thickness ( $D/t$ ) ratio have a larger influence on axial load capacity ( $N_{exp}/N_{cal}$ ). This trend is more remarkable in the  $\bar{a} = 1.842$ ,  $L_k/D = 12$  than other non-dimensional width-to-thickness ratio ( $\bar{a}$ ). The yield strength ( $F_y$ ) of the steel tube does seem to have a significant influence on axial load capacity ( $N_{exp}/N_{cal}$ ) or non-dimensional width-to-thickness ( $\bar{a}$ ) ratio.

3) AISC provisions underestimate the ultimate axial load capacity ( $N$ ) for the compression member of an HCFT column with equal sectional areas. In the case of  $D/t = 23.4$  and  $L_k/D = 4$ , the underestimate is  $N_{AJJ}$ , Nm of 95.7%,  $N_T$  of 91.5% with waste of sectional area. A design subject to AISC provisions requires more than from 4.3 to 8.5% sectional areas, in the same load conditions. Also, for  $L_k/D = 12$  and  $D/t = 23.4$ , it is estimated  $N_{AJJ}$  of 94.9%,  $N_m$  of 96.9% and  $N_T$  of 91.5% are waste. This requires from 3.1 to 8.5% more sectional area.

4) In selecting concrete for CFT, when a high-strength steel tube is used to prevent prior crushing of concrete in an ultimate state, low strength concrete is not recommended.

5) An exact solution of the elasto-plastic bending moment ( $M$ )-curvature ( $\phi$ ) of a sectional member of square steel tube is drawn by considering elasto-plastic and strain hardening ranges. When the specimen attain to the strain hardening range via the elasto-plastic area, the trend is toward a decrease in bending moment ( $M$ ) and ultimate axial load capacity ( $N$ ), with an increment of the curvature ( $\phi$ ) and axial load capacity ratio ( $S_0$ ) in analytical and experimental results. Therefore, it is estimated that an appropriate selection of width-to-thickness ratio ( $D/t$ ) improves ultimate axial load capacity ( $N$ ) and stiffness of the column. Deformational efficiency is improved in consideration of the high-strength concrete for CFT column, when the high axial load capacity ratio ( $S_0$ ), the deflection ( $\delta$ ) and the buckling of compressive flange and that of the web is minimized. The axial load ( $N$ )-bending moment ( $M$ ) capacity and the bending moment ( $M$ )-curvature ( $\phi$ ) of HCFT columns can be predicted with reasonable accuracy using the proposal formula for high-strength concrete CFT columns. The bending moment ( $M$ )-curvature ( $\phi$ ) of HCFT columns could be conservatively predicted by using the proposal formula. The proposal formula methods gave closer predictions of the test results than the current code provisions, and thus are acceptable for the calculation of the axial load capacity ( $S_0$ ) ratio, the width to thickness ( $D/t$ ) ratio.

## Acknowledgements

This work was supported by the Korea Research Foundation Grant (KRF-2005-D00181).

## References

- ACI Committee 318, (2005), Building code requirements for reinforcement concrete and commentary. American Concrete Institute: 119-124.
- AISC. (2005), *Load and resistance factor design (LRFD) specification for structural steel buildings*, Chicago IL: American Institute of Steel Construction, Inc: 77-83.
- Architectural Institute of Japan, (1997), *Recommendations for design and construction of concrete filled steel tubular structures*: 34-68.
- Architectural Institute of Japan, (1975), *Recommendations for plasticity design of steel structures*: 114-129.
- Architectural Institute of Japan, (1987), *Standard for structural calculation of steel reinforced concrete structures*.
- Architectural Institute of Korea (2004), *Standard for design and construction of concrete filled steel tubular structures*, Seoul Korea: 24-34.
- Campione G and Scibilia N. (2002), "Beam-column behavior of concrete filled steel tubes", *Steel Compos. Struct.*, **2**(4): 259-276
- Eurocode 4(EC4, 1994), *European Committee for Standardization (draft: Design of composite steel and concrete structures)*.
- Han, L.H. and Yao, G.H. (2003), "Influence of concrete compaction on the strength of concrete-filled steel RHS columns", *J. Constr. Steel Res.*, **59**(6), 751-767.
- Inai, E., Mukai, A., Kai, M., Tokinoya, H., Fukumoto, T. and Mori, K. (2004), "Behavior of concrete-filled steel tube beam columns", *ASCE* February; **130**(2), 189-202.
- Inoue, T., Fukumoto, T., Hayashi, N., and Okada, T. (1994), "Shear-flexural behavior of concrete filled steel tubular column using high-strength materials", *Summary of Technical papers of Annual Meeting of Architectural Institute of Japan, Structures II*, Architectural Institute of Japan, Tokyo, **1994**, 1599-1600.
- Itoh, S. and Yauzaki, C. (1992), "Studies on resistance and deformation capacities of concrete-filled with low YR high-tensile steel and high-strength concrete", *Summary of Technical papers of Annual Meeting of Architectural Institute of Japan, Structures II*, Architectural Institute of Japan, Tokyo, 1801-1802.

- Knowles, R. B. and Park, R. (1969), "Strength of concrete filled steel tubular column", *J. Struct. Div., ASCE*; 95(ST12), 2565-87.
- Lee, S.J., Park, J.M., and Kim W.J. (2000), "Behavior properties of high-strength concrete filled steel tube columns", *3<sup>rd</sup> international symposium on architectural interchanges in Asia*, AIA February: 923-934.
- Lee, S.J., Park, J.M., and Kim W.J. (1998), "A study on behaviors of high-performance concrete filled steel tube column using silica-fume", *Pacific structural steel conference*, PSSC October: 949-954.
- Liu, D., Gho, W. M. and Yuan, J. (2003), "Ultimate capacity of high-strength rectangular concrete-filled steel hollow section stub columns", *J. Constr. Steel Res.*, **59**(12), 1499-515.
- Popovics s. (1973), "A numerical approach to the complete stress-strain curves for concrete", *Cement and Concrete Res.*, **3**(5), 583-599.
- Saito, Y., Yamaguchi, I., Matsutani, T., Kadono, A., and Matsumura, H. (1989), "A study on the behavior of concrete filled steel tubular columns", Part 1—6. *Summary of Technical papers of Annual Meeting of Architectural Institute of Japan, Structures II*, Architectural Institute of Japan, Tokyo, 1613-1624.
- Sakino, K., Nakahara, H., Morino, S. and Nishiyama, I. (2004), "Behavior of centrally loaded concrete-filled steel-tube short columns", *J. Struct. Eng., ASCE*; **130**(2), 180-188.
- Shams, M. and Saadeghvaziri, M. A. (1999), "Nonlinear response of concrete-filled steel tubular columns under axial loading", *ACI Struct. J.*, **96**(5), 1009-17.
- Takanori SATO. (1999), "Proposal of unified and simplified design method for concrete filled steel tube in short column to slender column", *AIJ J. Struct. Constr. Eng.*, December, **526**, 209-219.
- Tomii, M., Yashimaro, K. and Morishita, Y. (1977), "Experimental studies on concrete filled steel tubular stub columns under concentric loading", *Proceedings of the International Colloquium on Stability of Structures under Static and Dynamic Loads*. Washington; SSRC/ASCE: 718-41.
- Uy, B. (2003), "High-strength steel-concrete composite columns for buildings", *Struct. Build.*, **156**, 3-14.
- Varma, A. H., Ricles, J. M., Sause, R., Ream, A., Sause, R., and Lu, L. W. (2004), "Seismic behavior and design of high-strength square concrete-filled steel tube beam columns", *J. Struct. Eng., ASCE* February 2004, **130**(2), 169-179.
- Young, B. and Lui, W. M. (2005), "Behavior of cold-formed high strength stainless steel sections", *J. Struct. Eng.*, ASCE, **131**(11), 1738-1745.

## Nomenclature

$A_{sr}$	Area of continuous reinforcing bars
$Elo$	Elongation
$El_{eff}$	Effective stiffness of composite section
$F_{max}$	Tension strength of steel
$F_{yr}$	Specified minimum yield stress of reinforcing bars
$K$	Effective length factor
$M_{AS}$	Maximum yield moment capacity
${}_cM_u$	Ultimate moment capacity of filled concrete slender column
${}_sM_u$	Ultimate moment capacity of steel tube slender column
${}_sM_{u0}$	Ultimate moment capacity of case that steel tube receives moment
$N_{u1}$	Ultimate axial capacity of short column
$N_{u2}$	Ultimate axial capacity of calculation by
${}_cN_u$	Ultimate axial capacity of filled concrete slender column
${}_sN_u$	Ultimate axial capacity of steel tube slender column
$p_e$	Critical load
$p_n$	Nominal compressive strength
$p_o$	Nominal axial compressive strength without consideration of length effects
$\alpha_c$	Factors dependant on the compressive strength of concrete

CC